INSTITUTE OF PHYSICS PUBLISHING METROLOGIA
Metrologia **43** (2006) 247–258 doi:10.1088/0026-1394/43/3/007

Transport properties of argon at zero density from viscosity-ratio measurements

Eric F May[1,2], **Michael R Moldover**[1,3], **Robert F Berg**[1] **and John J Hurly**[1]

[1] Process Measurements Division, National Institute of Standards and Technology Gaithersburg, MD 20899-8360, USA
[2] School of Oil & Gas Engineering, University of Western Australia, Crawley, WA 6009, Australia

E-mail: michael.moldover@nist.gov

Received 20 January 2006
Published 6 April 2006
Online at stacks.iop.org/Met/43/247

Abstract
We determined the zero-density viscosity $\eta^{\mathrm{Ar}}_{0,\mathrm{T}}$ and thermal conductivity $\lambda^{\mathrm{Ar}}_{0,\mathrm{T}}$ of argon with a standard uncertainty of 0.084% in the temperature range 200 K to 400 K. This uncertainty is dominated by the uncertainty of helium's viscosity $\eta^{\mathrm{He}}_{0,\mathrm{T}}$, which we estimate to be 0.080% based upon the difference between *ab initio* and experimental values at 298.15 K. Our results may improve (1) the argon–argon interatomic potential, (2) calculated boundary-layer corrections for primary acoustic thermometry, and (3) calibrations of laminar flow meters as well as instruments for measuring transport properties. At 298.15 K, we determined the ratio $\eta^{\mathrm{Ar}}_{0,298}/\eta^{\mathrm{He}}_{0,298} = 1.138\,00 \pm 0.000\,13$ from measurements of the flow rate of these gases through a quartz capillary while simultaneously measuring the pressures at the ends of the capillary. Between 200 K and 400 K, we used a two-capillary viscometer to determine $\eta^{\mathrm{Ar}}_{0,\mathrm{T}}/\eta^{\mathrm{He}}_{0,\mathrm{T}} = 1.211\,67 - 0.820\,34\exp(-T/123.78\,\mathrm{K})$ with an uncertainty of 0.024%. From $\eta^{\mathrm{Ar}}_{0,\mathrm{T}}/\eta^{\mathrm{He}}_{0,\mathrm{T}}$, we computed $\eta^{\mathrm{Ar}}_{0,\mathrm{T}}$ using the values of $\eta^{\mathrm{He}}_{0,\mathrm{T}}$ calculated *ab initio*. Finally, we computed the thermal conductivity of argon from $\eta^{\mathrm{Ar}}_{0,\mathrm{T}}$ and values of the Prandtl number that we computed from argon–argon interatomic potentials.

1. Introduction

Argon-based, primary acoustic thermometry and acoustic redeterminations of the universal gas constant require accurate values of the thermal conductivity $\lambda^{\mathrm{Ar}}_{0,\mathrm{T}}$ of low-density argon [1–4]. These needs motivated us to determine $\lambda^{\mathrm{Ar}}_{0,\mathrm{T}}$ by combining experimental and theoretical viscosity data for helium, experimental data for the ratio of the viscosity of argon to the viscosity of helium, and theoretical values for the Prandtl number for argon. The uncertainty of $\lambda^{\mathrm{Ar}}_{0,\mathrm{T}}$ determined by this method is smaller than the uncertainty of direct measurements of the thermal conductivity. (The notation uses a superscript to denote the gas; the first subscript is the pressure, and the second subscript is the kelvin temperature.)

[3] Author to whom any correspondence should be addressed.

We started with a reference value for the viscosity of helium at zero density and 298 K ($\eta^{\mathrm{He}}_{0,298}$) deduced from the best experimental data and the best value calculated *ab initio*. As the temperature departs from 298 K, the uncertainty of the ratio $(\eta^{\mathrm{He}}_{0,\mathrm{T}}/\eta^{\mathrm{He}}_{0,298})_{\mathrm{ab\,initio}}$, as calculated *ab initio*, grows more slowly than the uncertainty of the measurements; therefore, we used the *ab initio* values of $(\eta^{\mathrm{He}}_{0,\mathrm{T}}/\eta^{\mathrm{He}}_{0,298})_{\mathrm{ab\,initio}}$ as references at other temperatures. We obtained the viscosity of argon $\eta^{\mathrm{Ar}}_{0,\mathrm{T}}$ with the small relative standard uncertainty of 0.084% from the expression

$$\eta^{\mathrm{Ar}}_{0,\mathrm{T}} = \eta^{\mathrm{He}}_{0,298}\left(\frac{\eta^{\mathrm{He}}_{0,\mathrm{T}}}{\eta^{\mathrm{He}}_{0,298}}\right)_{\mathrm{ab\,initio}}\left(\frac{\eta^{\mathrm{Ar}}_{0,298}}{\eta^{\mathrm{He}}_{0,298}}\right)R^{\mathrm{Ar,He}}_{\mathrm{T},298}. \qquad (1)$$

Equation (1) has four factors: (1) our reference value $\eta^{\mathrm{He}}_{0,298}$ for helium's viscosity, (2) the temperature-dependent

ratio $(\eta^{He}_{0,T}/\eta^{He}_{0,298})_{ab\,initio}$ calculated *ab initio* from quantum mechanics and statistical mechanics [5, 6], (3) the argon–helium viscosity ratio $\eta^{Ar}_{0,298}/\eta^{He}_{0,298}$ that we measured at 298.15 K, and (4) our measurements of the temperature-dependent ratio of viscosity ratios,

$$R^{Ar,He}_{T,298} \equiv \left(\frac{\eta^{Ar}_{0,T}}{\eta^{He}_{0,T}}\right) \Big/ \left(\frac{\eta^{Ar}_{0,298}}{\eta^{He}_{0,298}}\right). \tag{2}$$

We then obtained the thermal conductivity from

$$\lambda^{Ar}_{0,T} = \frac{5R}{2}\frac{\eta^{Ar}_{0,T}}{M\,Pr^{Ar}_{0,T}}. \tag{3}$$

Equation (3) contains the ideal-gas molar heat capacity of argon $C_p = 5R/2$, where R is the universal gas constant, the molar mass M, and the Prandtl number $Pr \equiv \eta C_p/(\lambda M)$ that we calculated from argon–argon interatomic potentials. The uncertainty of $\lambda^{Ar}_{0,T}$ computed from equation (3) is smaller than the uncertainty of direct measurements of the thermal conductivity.

We combined two approaches to measure viscosity ratios. First, we determined the reference ratio $\eta^{Ar}_{0,298}/\eta^{He}_{0,298} = 1.138\,00 \pm 0.000\,13$ by measuring the flow rate of helium and argon through single quartz capillaries at 298.15 K while measuring the pressures at the ends of the capillary. Then, we measured the ratio of viscosity ratios $R^{Ar,He}_{T,298}$ in the temperature range 200 K $< T <$ 400 K without additional, manual, flow-rate measurements by using the automated, two-capillary viscometer sketched in figure 1. The upstream capillary was thermostatted at 298.15 K; the downstream capillary was thermostatted at test temperatures T. We alternately flowed helium and argon through the two-capillary viscometer while measuring the pressures at the ends of both capillaries. Combining the results from the two-capillary viscometer with those from the single-capillary viscometer produced the argon–helium viscosity ratio $\eta^{Ar}_{0,T}/\eta^{He}_{0,T}$ with the temperature dependence

$$\eta^{Ar}_{0,T}/\eta^{He}_{0,T} = 1.211\,67 - 0.820\,34\exp(-T/123.78\,\mathrm{K});$$
$$200\,\mathrm{K} < T < 400\,\mathrm{K} \tag{4}$$

and the small relative uncertainty of 0.024%. The rms deviation of the data from equation (4) was 0.005%.

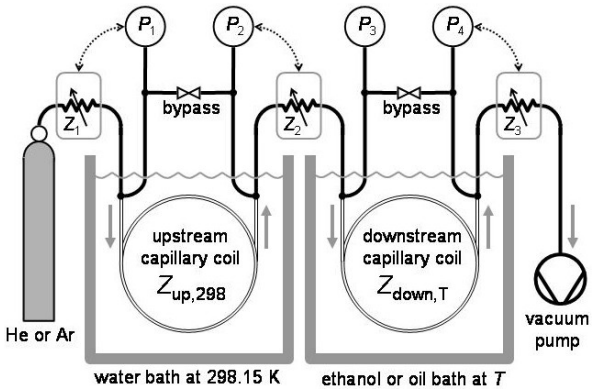

Figure 1. Schematic diagram of the two-capillary viscometer. The impedances Z_{up} and Z_{down} were coiled nickel capillaries with a length of 7 m and an inside diameter of 0.8 mm. The variable impedances Z_1 and Z_3 were piezoelectric gas leak valves and Z_2 was either a leak valve or a mass flow controller.

Frequently, gas viscometry has used careful measurements of the viscosity of nitrogen as a standard. In contrast, we used the viscosity of helium calculated *ab initio* as a viscosity standard. At zero density, the uncertainty claimed for the *ab initio* value [5, 6] is comparable to the uncertainty claimed for the most accurate measurements [7–10]. As one departs from the ambient temperature, the uncertainty advantage of the helium standard grows because measurement uncertainties grow faster than those of the *ab initio* values [5].

The recently revised *ab initio* value at 298.15 K [6] and the most accurate measured value [10] disagree by twice their combined uncertainty. We therefore anchored the *ab initio* temperature-dependent ratio $(\eta^{He}_{0,T}/\eta^{He}_{0,298})_{ab\,initio}$ to the reference value $\eta^{He}_{0,298} = (19.833 \pm 0.016)$ μPa s that encompasses both values. The uncertainty of our results for $\eta^{Ar}_{0,T}$ and $\lambda^{Ar}_{0,T}$ is dominated by the uncertainty of the reference value (see table 1). If more accurate *ab initio* calculations reduce the uncertainty of the reference value, we will recalculate $\eta^{Ar}_{0,T}$ and $\lambda^{Ar}_{0,T}$ from the present ratio measurements with a reduced uncertainty.

We are not aware of any precedent for our use of the calculated viscosity of helium as a standard for viscosity ratio measurements. However, there are many precedents for our viscosity ratio measurements; we cite several. Around 1970, the advantages of measuring viscosity ratios were widely appreciated and applied to many gases over very wide temperature ranges [11–16]. For example, Camani [16] used a four-capillary differential viscometer to measure the difference between the viscosities of ortho-hydrogen and para-hydrogen with the remarkable resolution of 0.004%. Today, a group at Loughborough University and the University of Strathclyde is using viscosity-ratio measurements to measure the change in the viscosity of a gas upon the addition of an impurity [17].

Table 1. Contributions to the uncertainty of the transport properties of argon.

Source	Relative standard uncertainty	Estimator	Section
Reference value $\eta^{He}_{0,T}$	0.000 80	Inconsistency of *ab initio* and measured values	2.3
Ab initio ratio $\eta^{He}_{0,T}/\eta^{He}_{0,298}$	0.000 06	Differences among He potentials	2.3
Reference ratio $\eta^{Ar}_{0,298}/\eta^{He}_{0,298}$	0.000 11	Scatter of data; helium slip correction	3.1
Dependence of $R^{Ar,He}_{T,298}$ on De	0.000 17	Extrapolation to zero Dean number	4.3
Scatter in $R^{Ar,He}_{T,298}$	0.000 05	Scatter of pressure difference data	Figure 4
Argon viscosity virial	0.000 10	Spread among literature measurements	4.2
Argon Prandtl number	0.000 04	Differences among argon potentials	6
Root sum of squares	0.000 84		

The remainder of this manuscript is organized as follows. Section 2 outlines the principles of the measurements and discusses the uncertainty of the viscosity of helium. Section 3 describes the apparatus and the procedures. Section 4 describes the analysis of the two-capillary viscometer data. Section 5 includes a performance test of the two-capillary instrument and compares the present viscosity ratio data with results from the literature. The uncertainties of the present results are small enough to distinguish among various models for the argon–argon interatomic potential. In particular, the present results are in better agreement with the Boyes potential [18] than with the more frequently cited potential Aziz [19] generated at about the same time. Section 6 discusses the small uncertainty of the Prandtl number and the calculation of the thermal conductivity of argon. In section 7, we show that our results for $\eta_{0,\mathrm{T}}^{\mathrm{Ar}}$ and $\lambda_{0,\mathrm{T}}^{\mathrm{Ar}}$ are consistent with a recent, comprehensive review [20] of the transport properties of argon; however, the present results have much smaller uncertainties.

2. Principles of the measurements

2.1. The hydrodynamic model

We used the hydrodynamic model developed by Berg [9], who measured the pressures just upstream (p_1) and downstream (p_2) of a coiled capillary while gas flowed through the capillary at various, accurately measured, molar flow rates $\dot{n}$. Berg applied Poiseuille's law to a compressible fluid to derive the equation

$$\dot{n} = \frac{(p_1^2 - p_2^2)}{Z_{\mathrm{T}} \eta_{0,\mathrm{T}}^{\mathrm{gas}} RT} C^{\mathrm{gas}}(T, p_1, p_2), \tag{5}$$

with the definitions

$$Z_T \equiv 16L/(\pi r^4) \tag{6}$$

and

$$C^{\mathrm{gas}}(T, p_1, p_2) \equiv \left(1 + \sum_{i=1}^{5} c_i^{\mathrm{gas}}\right) f_{\mathrm{cent}}(De, r/R_{\mathrm{coil}}). \tag{7}$$

Here, r, L, and R_{coil} are, respectively, the bore radius, length, and radius of curvature of the capillary coil, and Z_T is the capillary's (fluid-independent) impedance at the temperature T. In equation (7), the five terms c_i^{gas} are small corrections to Poiseuille's law for the flow of an ideal gas through a straight capillary. They account for (1) the density virial coefficients B_ρ and C_ρ and the viscosity virial coefficient B_η, (2) the slip at the capillary wall, (3) the increase in the kinetic energy of the gas as it enters the capillary, (4) the gas expansion along the length of the capillary, and (5) the radial temperature distribution within the gas resulting from gas expansion and viscous dissipation. In equation (7), the function f_{cent} accounts for the centrifugal effect due to coiling of the capillary. Reference [9] provides explicit forms for the c_i and for f_{cent}. Here, $De \equiv (r/R_{\mathrm{coil}})^{1/2} Re$ is the Dean number; $Re \equiv 2M\dot{n}/(\pi r \bar{\eta})$ is the Reynolds number; M is the molar mass, and $\bar{\eta}$ is the viscosity at an average pressure defined by equation (7) of [9].

Berg tested the understanding of the correction terms by conducting flow measurements in the ranges: 30 kPa $< p_2 < p_1 <$ 300 kPa; $0 < Re < 1200$, $0 < De < 66$, and $0 < Kn < 0.002$. Here $Kn \equiv \lambda_{1/2}/r$ is the Knudsen number, and $\lambda_{1/2}$ is the mean free path for the gas molecules at pressure $(p_1 + p_2)/2$. Remarkably, Berg's result $\eta_{0,298}^{\mathrm{He}} = (19.842 \pm 0.007)\,\mu\mathrm{Pa\,s}$ [10] for the viscosity of helium at 298.15 K differed from Hurly and Moldover's revised *ab initio* value $\eta_{0,298}^{\mathrm{He}} = (19.823 \pm 0.007)\,\mu\mathrm{Pa\,s}$ [6] by only 0.10%, or twice the combined standard uncertainty. Thus, coiled capillary flow meters are well understood when the pressure, the Reynolds number, the Knudsen number and the Dean number are all within experimentally useful bounds. Even if the 0.10% difference had been caused solely by an unknown measurement error, the corresponding error of the present ratio measurements would be negligible.

2.2. Viscosity ratios

Figure 1 shows the two-capillary viscometer that we used to measure relative viscosity ratios. We denote the impedance of the upstream capillary, which was maintained at the reference temperature 298.15 K, by $Z_{\mathrm{up},298} \equiv 16L_{\mathrm{up},298}/(\pi r_{\mathrm{up},298}^4)$. In analogy, we denote the impedance of the downstream capillary at the test temperature T by $Z_{\mathrm{down,T}}$. We operated the two-capillary viscometer in two modes that we call (1) the flow-meter mode and (2) the helium-standard mode.

2.2.1. Flow-meter mode. In the flow-meter mode, the upstream capillary acted as an uncalibrated but highly reproducible flow meter. (Calibration requires at least a single, accurate, flow measurement.) While the argon flows through both capillaries, p_1 and p_2 are maintained at constant, predetermined values by controlling the impedances Z_1 and Z_2. Thus, the flow meter maintains a constant, unknown gas flow rate that is identical through both capillaries. If the time-averaged molar flow rate $\langle\dot{n}\rangle$ and the impedance Z_{down} were known, the downstream capillary could determine the viscosity at the temperature T using equation (5) and accurate measurements of p_3 and p_4. Since $\langle\dot{n}\rangle$ and Z_{down} are unknown, we apply equation (5) separately to the upstream and downstream capillaries and eliminate $\langle\dot{n}\rangle$ to obtain the 'flow-meter mode' working equation:

$$\frac{\eta_{0,\mathrm{T}}^{\mathrm{Ar}}}{\eta_{0,298}^{\mathrm{Ar}}} = \left[\frac{(p_3^2 - p_4^2)}{(p_1^2 - p_2^2)} \frac{C^{\mathrm{Ar}}(T, p_3, p_4)}{C^{\mathrm{Ar}}(298.15\,\mathrm{K}, p_1, p_2)}\right] \times \frac{298.15\,\mathrm{K}}{T} \frac{Z_{\mathrm{up},298}}{Z_{\mathrm{down},298}} \left(1 + 3\frac{\Delta L(T)}{L}\right). \tag{8}$$

This expression for the viscosity ratio requires two kinds of auxiliary data: (1) the thermal expansion $\Delta L(T)/L$ of the downstream capillary between 298.15 K and T and (2) the impedance ratio $Z_{\mathrm{up},298}/Z_{\mathrm{down},298}$. We obtained the thermal expansion from the literature [21], and we obtained $Z_{\mathrm{up},298}/Z_{\mathrm{down},298}$ by applying equation (8) to data taken while both capillaries were maintained at 298.15 K.

The flow-meter mode requires that the impedance ratio $Z_{\mathrm{up},298}/Z_{\mathrm{down},298}$ and the calibrations of the pressure gauges be stable during the intervals (weeks) between calibrations. Unfortunately, the impedance ratio increased from 1.000 05 to 1.000 44 during an interval of five months, perhaps because oil or particles accumulated in the upstream capillary. The

requirements for long term stability are relaxed in the helium-standard mode of operation, which makes it an attractive alternative to the flow-meter mode.

2.2.2. Helium-standard mode. In the helium-standard mode, the impedance ratio $Z_{\mathrm{up},298}/Z_{\mathrm{down,T}}$ is determined when needed by flowing helium through the instrument just before or just after the argon flows through the instrument. In effect, this procedure replaces the assumption of long term stability of the impedance ratio $Z_{\mathrm{up},298}/Z_{\mathrm{down},298}$ with the viscosity ratio $\eta^{\mathrm{He}}_{0,\mathrm{T}}/\eta^{\mathrm{He}}_{0,298}$. (The uncertainty of $\eta^{\mathrm{He}}_{0,\mathrm{T}}/\eta^{\mathrm{He}}_{0,298}$ is discussed in section 2.3.2.) We apply equation (8) twice, once to argon and then to helium, and divide the results to obtain the 'helium-standard mode' working equation:

$$R^{\mathrm{Ar,He}}_{\mathrm{T},298} = \frac{(p_3^2 - p_4^2)^{\mathrm{Ar}}}{(p_1^2 - p_2^2)^{\mathrm{Ar}}} \frac{(p_1^2 - p_2^2)^{\mathrm{He}}}{(p_3^2 - p_4^2)^{\mathrm{He}}} \frac{C^{\mathrm{Ar}}(T, p_3, p_4)}{C^{\mathrm{He}}(T, p_3, p_4)} \times \frac{C^{\mathrm{He}}(298.15\,\mathrm{K}, p_1, p_2)}{C^{\mathrm{Ar}}(298.15\,\mathrm{K}, p_1, p_2)}. \quad (9)$$

The dimensions of the capillaries appear only in the correction terms of equation (9); therefore, approximate values of the dimensions are sufficient.

We used the *variable* impedances Z_1 and Z_2 (figure 1) to maintain p_1 and p_2 at constant, identical values when both helium and argon flowed through the two capillaries. Although the two gases flowed at slightly different rates through the apparatus, this scheme has the benefit that the $(p_1^2 - p_2^2)$ terms drop out of equation (9). We also used the *variable* impedances Z_2 and Z_3 to achieve several different values of p_2 and p_4; data taken at several average pressures and at several flow rates were used to verify that the flow was well described by the hydrodynamic model. Consequently, the ratio measurements required several hours at each temperature as the apparatus stepped through two identical sets of $\{p_2, p_4\}$ values, first for helium and then for argon, or vice-versa.

The uncertainty contributed by the pressure measurements in the helium-standard mode can be identified by eliminating the $(p_1^2 - p_2^2)$ terms from equation (9) and ignoring the correction terms to obtain an approximate equation:

$$R^{\mathrm{Ar,He}}_{\mathrm{T},298} \approx \frac{(p_3 - p_4)^{\mathrm{Ar}}(p_3 + p_4)^{\mathrm{Ar}}}{(p_3 - p_4)^{\mathrm{He}}(p_3 + p_4)^{\mathrm{He}}}. \quad (10)$$

In equation (10), the pressure-difference ratio $(p_3 - p_4)^{\mathrm{Ar}}/(p_3 - p_4)^{\mathrm{He}}$ is the major contributor to the uncertainty of $R^{\mathrm{Ar,He}}_{\mathrm{T},298}$. Increasing the pressure differences will decrease this contribution, but only if the flow-dependent correction terms remain small. We reduced the uncertainty in the pressure-difference ratio by correcting for the relative zero drifts of the two pairs of transducers monitoring $\{p_1, p_2\}$ and $\{p_3, p_4\}$. To do so, we 'tared' the zeros just before and just after every flow measurement by closing isolation valves (not shown in figure 1) between the transducers and the viscometer and opening bypass valves connecting the transducer pairs. The apparent values of $(p_3 - p_4)$ and $(p_1 - p_2)$ in this tare state (at the average pressures of the measurement) were used to correct the pressure differences recorded when gas flowed through the capillaries. Due to partial cancellation within the pressure-sum ratio $(p_3 + p_4)^{\mathrm{Ar}}/(p_3 + p_4)^{\mathrm{He}}$, the uncertainty of $R^{\mathrm{Ar,He}}_{\mathrm{T},298}$ is smaller than the relative uncertainties of the individual values of p_3 and p_4. The uncertainty of $(p_3 - p_4)^{\mathrm{Ar}}/(p_3 - p_4)^{\mathrm{He}}$ was less than 0.01%; it was dominated by the instability (≈2 Pa) of the uncontrolled pressure p_3.

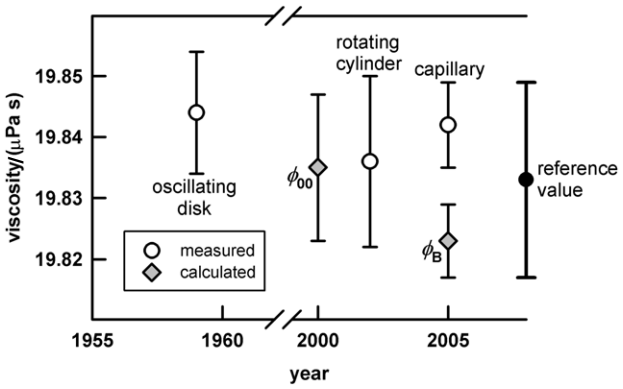

Figure 2. Accurate determinations of the viscosity of helium in the limit of zero pressure at 298.15 K. Kestin and Leidenfrost used an oscillating disc [7], Evers *et al* used a rotating cylinder [8], and Berg used a quartz capillary [9, 10]. In 2005, Hurly and Moldover [6] used the model potential ϕ_{B} to revise the *ab initio* value obtained in 2000 with the model potential ϕ_{00} [5].

To achieve small uncertainties in $(p_3 - p_4)^{\mathrm{Ar}}/(p_3 - p_4)^{\mathrm{He}}$, it was necessary to maintain stable flow-rates $\dot{n}$, which, in turn, required stable temperatures because $\dot{n}$ varies as $(\eta T)^{-1}$ when the entrance and exit pressures are fixed. As an example, consider argon, for which $\eta T \propto (T/\mathrm{K})^{1.87}$. To achieve an instability as small as $10^{-4}\dot{n}$, a fractional temperature instability of $10^{-4}T/1.87$ or less is required. (This corresponds to 11 mK at 200 K.) We achieved temperature stability by immersing each capillary in its own well-stirred, thermostatted bath.

2.3. Viscosity of helium

Equation (1) requires a reference value for the viscosity of helium at zero density and 298 K ($\eta^{\mathrm{He}}_{0,298}$). In this section, we obtain the reference value and its uncertainty by examining the best measurements and the best values calculated *ab initio*. Equation (1) also requires values of $(\eta^{\mathrm{He}}_{0,\mathrm{T}}/\eta^{\mathrm{He}}_{0,298})_{\mathrm{ab\,initio}}$. For this ratio, we use *ab initio* values instead of measured values because the uncertainty of the *ab initio* values grows more slowly than the uncertainty of measurements as the temperature departs from 298 K. In the present temperature range, the fractional uncertainty of $(\eta^{\mathrm{He}}_{0,\mathrm{T}}/\eta^{\mathrm{He}}_{0,298})_{\mathrm{ab\,initio}}$ is smaller than the fractional uncertainty of $(\eta^{\mathrm{He}}_{0,\mathrm{T}})_{\mathrm{ab\,initio}}$.

2.3.1. Viscosity of dilute helium at 298.15 K: $\eta^{\mathrm{He}}_{0,298}$. In this section we discuss the value and uncertainty of $\eta^{\mathrm{He}}_{0,298}$, the viscosity of helium in the limit of zero pressure at 298.15 K. Figure 2 shows selected primary measurements of $\eta^{\mathrm{He}}_{0,298}$. In 1959, Kestin and Leidenfrost [7] used an oscillating disc viscometer to measure the viscosity of helium at 20 °C. (The value in figure 2 is adjusted to 298.15 K.) During the next 40 years, all accurate measurements of helium's viscosity were made with viscometers calibrated with respect to the viscosity values of [7], which had a claimed uncertainty of 0.05%. The first accurate measurement that was independent of [7] was in 2002 by Evers *et al* [8], who used a rotating cylinder to obtain

a relative uncertainty of 0.07%. In 2005, Berg [9, 10] used a quartz capillary to obtain a relative uncertainty of 0.04%.

Also shown in figure 2 are values of helium's viscosity calculated *ab initio* from quantum mechanics and statistical mechanics. In the year 2000, Hurly and Moldover [5] tabulated *ab initio* values of $\eta^{\mathrm{He}}_{0,\mathrm{T}}$ that they had calculated using the model $\varphi_{00}(r)$ of the He–He interatomic potential $\phi(r)$. Their calculation began with theoretical 'data', i.e. values of $\varphi(r)$ calculated by several research groups at discrete values of r. The uncertainty of their results came from two sources: (1) the data from different research groups were inconsistent, and (2) the functional form used to fit the theoretical data was not known. To estimate the effects of these sources, Hurly and Moldover used six model potentials to represent $\varphi(r)$ data at several levels of approximation. Three potentials (φ_{00}, φ_{A}, φ_{B}, in their notation) were fitted to different consistent subsets among the inconsistent data. Four potentials (φ_{A}, $\varphi_{\mathrm{A}+}$, $\varphi_{\mathrm{A}-}$, φ_{SAPT}) used different functions to fit a particular subset of the *ab initio* data. (The functional forms of φ_{A} and φ_{SAPT} differ. The forms of φ_{A}, $\varphi_{\mathrm{A}+}$ and $\varphi_{\mathrm{A}-}$ are identical. This form was used three times, once to fit the data to obtain φ_{A}, then twice to obtain $\varphi_{\mathrm{A}+}$ and $\varphi_{\mathrm{A}-}$ by fitting the data plus and minus their claimed uncertainty bounds.)

We use the upper panel of figure 3 to discuss contributions to the uncertainty of *ab initio* values of $\eta^{\mathrm{He}}_{0,\mathrm{T}}$. In the range $200\,\mathrm{K} < T < 400\,\mathrm{K}$, the values of $\eta^{\mathrm{He}}_{0,\mathrm{T}}$ computed from the potentials (φ_{00}, φ_{A}, φ_{B}) span a fractional range of approximately 0.0006; the values computed from the potentials (φ_{A}, $\varphi_{\mathrm{A}+}$, $\varphi_{\mathrm{A}-}$, φ_{SAPT}) span the fractional range 0.0003. Thus, the uncertainty from the inconsistent sets of *ab initio* data is twice the uncertainty from fitting a particular subset with different functions that allow for the claimed uncertainty of the data.

Since the year 2000, there has been considerable progress in the values of $\varphi(r)$ for helium, *ab initio*. (See, for example, [22–24].) Some of the new *ab initio* data replace earlier data with the effect of greatly reducing the inconsistencies among the data. Also, a preliminary analysis of the new data indicates that the true He–He potential is much closer to the model potential φ_{B} than to the potential φ_{00} that was believed to be best in 2000 [6]. However, some uncertainty from fitting the data with diverse functions remains. Here, we use φ_{B} to calculate $\eta^{\mathrm{He}}_{0,\mathrm{T}}$ and we estimate that the fractional uncertainty of $\eta^{\mathrm{He}}_{0,\mathrm{T}}$ is 0.000 30.

Unfortunately, the revised *ab initio* value and the capillary measurement value disagree by twice their combined uncertainty of 0.05%, and the existence of a significant unidentified error seems likely. The simplest assumption is that only one of the values has such an error, so that its correction would bring it close to the other value. We therefore assign to the reference value $\eta^{\mathrm{He}}_{0,298}$ the intermediate value

$$\eta^{\mathrm{He}}_{0,298} = (19.833 \pm 0.016)\ \mu\mathrm{Pa\,s}. \qquad (11)$$

The relative standard uncertainty of 0.08% encompasses the standard uncertainties of the calculated and measured values. Equation (11) is consistent also with the oscillating disc measurement [7] and the rotating cylinder measurement [8].

2.3.2. Viscosity ratio of helium: $\eta^{\mathrm{He}}_{0,\mathrm{T}}/\eta^{\mathrm{He}}_{0,298}$. In the helium-standard mode, we used the *ab initio* viscosity ratio $\eta^{\mathrm{He}}_{0,\mathrm{T}}/\eta^{\mathrm{He}}_{0,298}$ to remove the requirement of knowing the impedance ratio $Z_{\mathrm{up},298}/Z_{\mathrm{down,T}}$. In this section we use the lower panel of figure 3 to estimate the uncertainty of $\eta^{\mathrm{He}}_{0,\mathrm{T}}/\eta^{\mathrm{He}}_{0,298}$ in the temperature range $200\,\mathrm{K} < T < 400\,\mathrm{K}$. The fractional uncertainty of the ratio $\eta^{\mathrm{He}}_{0,\mathrm{T}}/\eta^{\mathrm{He}}_{0,298}$ is much smaller than the fractional uncertainty of $\eta^{\mathrm{He}}_{0,\mathrm{T}}$ itself because the values of $\eta^{\mathrm{He}}_{0,\mathrm{T}}$ at nearby temperatures are highly correlated. The lower panel of figure 3 shows that the ratios $\eta^{\mathrm{He}}_{0,\mathrm{T}}/\eta^{\mathrm{He}}_{0,298}$ computed from the six potentials span a fractional range of only 0.000 09 and that the span of different fits to the same *ab intio* data (φ_{A}, $\varphi_{\mathrm{A}+}$, $\varphi_{\mathrm{A}-}$, φ_{SAPT}) is 0.000 06, or less. Thus, we estimate that the relative uncertainty of $\eta^{\mathrm{He}}_{0,\mathrm{T}}/\eta^{\mathrm{He}}_{0,298}$, as computed from φ_{B}, is 0.000 06 or less in the range $200\,\mathrm{K} < T < 400\,\mathrm{K}$.

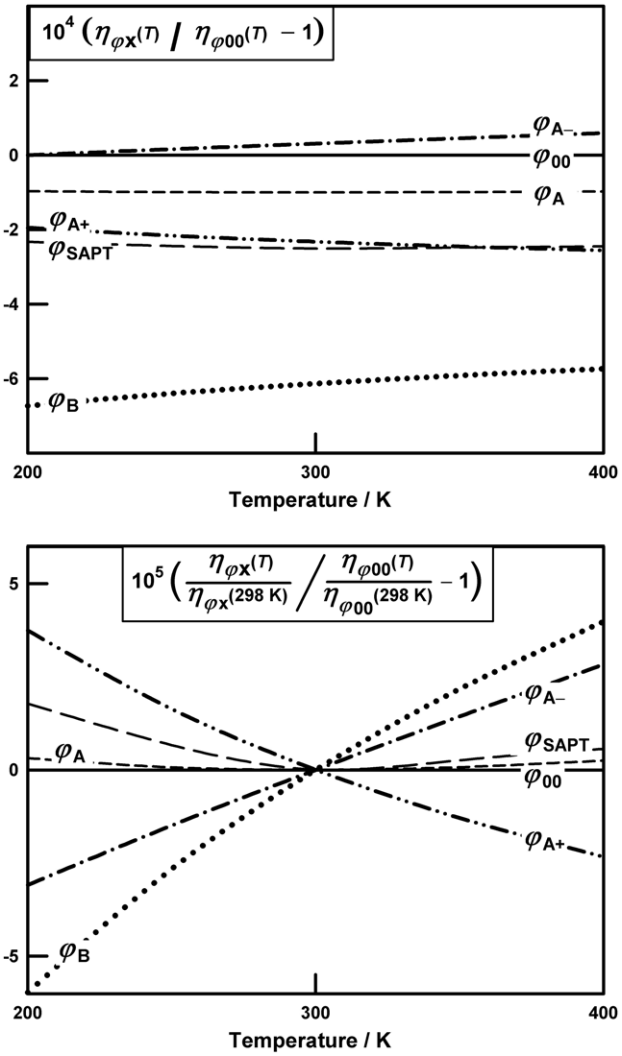

Figure 3. Top: an enlargement of figure 3 from [5]. The curves display the ratio of the viscosity computed using various He–He potentials to the viscosity computed from φ_{00} in [5]. Bottom: ratio of ratios. The temperature-dependent viscosity-ratio $\eta^{\mathrm{He}}_{0,\mathrm{T}}/\eta^{\mathrm{He}}_{0,298}$ computed from various potentials is divided by the same ratio computed using φ_{00}.

3. Apparatus, materials and procedures

3.1. Reference, single capillary measurements at 298.15 K

The measurements of the ratios $R^{\mathrm{Ar,He}}_{\mathrm{T},298}$ made with the two-capillary viscometer require at least one reference datum to

convert the ratios to values of $\eta^{\mathrm{Ar}}_{0,\mathrm{T}}/\eta^{\mathrm{He}}_{0,\mathrm{T}}$. We used the reference datum

$$\eta^{\mathrm{Ar}}_{0,298}/\eta^{He}_{0,298} = 1.138\,00 \pm 0.000\,13. \qquad (12)$$

Equation (12) is the average of two sets of measurements made at 298.15 K. The first set was made by Berg to determine the values of $\eta^{\mathrm{He}}_{0,298}$ and $\eta^{\mathrm{Ar}}_{0,298}$. He used a flow meter and a quartz capillary of accurately known dimensions [9]. His corrected result is $1.138\,07 \times (1 \pm 0.000\,16)$ [10]. Here, the relative uncertainty is the sum in quadrature of three terms: the adjusted relative uncertainties of $\eta^{\mathrm{He}}_{0,298}(0.000\,10)$ and $\eta^{\mathrm{Ar}}_{0,298}(0.000\,08)$ plus a term (0.000 10) that comes from the momentum accommodation K_{slip} of helium on the quartz capillary. The adjustments accounted for the uncertainty components that were common to both gases. The component for K_{slip} was not discussed in [9].

The second set of measurements of $\eta^{\mathrm{Ar}}_{0,298}/\eta^{\mathrm{He}}_{0,298}$ was made for this work. It used different thermometers, different (unthermostatted) pressure transducers, and a different (unthermostatted) quartz capillary, whose dimensions were known only approximately. The result was $1.137\,93 \times (1 \pm 0.000\,16)$. The uncertainty in equation (12) was estimated independent of the individual uncertainties by assuming that the two results sampled a normal distribution with an unknown standard deviation. The best estimate of the standard deviation of that normal distribution is the standard deviation of the two results multiplied by the factor 1.84 derived from Student's t distribution [25, 26].

3.2. Two-capillary viscometer

The two-capillary viscometer comprised two coils of electroformed nickel tubing, each with a nominal internal diameter of 0.762 mm, a length of approximately 7.45 m, and a coil curvature radius of 0.100 m. (The length and curvature radius were estimated using an ordinary ruler and tape.) The tubing was designed for gas chromatography, and the manufacturer claimed that it had an extremely smooth internal surface.

Each coiled capillary started and finished with a straight section approximately 10 cm long that terminated at a T-union. (The side branch of each union led to a pressure transducer.) The internal bore of the T-unions matched that of the capillary tube. This matching minimized the disruption of the flow by the union and allowed us to set the entrance correction term in equation (5) to zero. The first 20 cm of the tubing leading from the T-unions to the variable impedances (and to the pressure transducers) were the same as the tubing used for the capillaries. Thus, the parabolic flow profile was well established within the bore before the gas reached the coiled capillary.

The capillaries were wound 11.5 times around an aluminium cylinder to form a helix approximately 4 cm long and clamped in several places to prevent inadvertent unwinding. The axis of the capillary helix was horizontal. The straight sections at the ends of the capillary coils were oriented so that the T-unions were at the same height. An aluminium base plate mounted in a vertical plane supported each aluminium cylinder, the T-unions, the 20 cm long straight sections of tubing, and adapters that connected the nickel straight sections to stainless steel tubes that led to the pressure transducers and variable impedances.

Each base plate was immersed in the thermostatted bath. Approximately 1 m of each stainless steel tube was coiled so that it was also immersed in the bath. For helium and argon at flow rates $\leqslant 100\,\mu\mathrm{mol\,s^{-1}}$, the characteristic length for thermal equilibration with the bath was less than 10 cm.

The upstream, reference bath was maintained at 298.15 K. The design of this 60 L water-filled bath follows that of the much larger bath described by Wright *et al* [27]. The temperature fluctuations and inhomogeneities were less than ±2 mK. The downstream bath was a stainless steel Dewar similar to the one described by Wilhelm *et al* [28]. Below 300 K, it was filled with 25 L of ethanol; above 300 K, it was filled with silicone oil. When this bath was well above or well below the ambient temperature, the temperature fluctuations and inhomogeneities were of the order of 0.01 K as determined by moving a thermometer. The temperature of each bath was monitored with a long-stem, standard platinum resistance thermometer. Far from the ambient temperature, the uncertainty of the tabulated temperatures was approximately 0.01 K.

The pressure transducers measuring p_1, p_2 and p_3 had a span of 300 kPa. The transducer monitoring p_4 had a span of 150 kPa, and at the start of these measurements the manufacturer's calibration was still valid. The manufacturer claimed an uncertainty of 0.008% of full scale (±12 Pa). We measured all four pressures with a resolution of 0.16 Pa. An intercomparison of the four transducers was conducted several times over the course of six months. A significant change was found on only one occasion: a −9 Pa shift of p_3 that was removed by taring. Furthermore, over the range of 12 kPa to 150 kPa, the slopes of the four transducers remained consistent within 4×10^{-5}.

Each pair of pressure transducers ($\{p_1, p_2\}$ and $\{p_3, p_4\}$) was housed in a thermostatted enclosure similar to the air bath described by Berg [29]. Each enclosure also housed a bypass valve that was used to tare the transducer pair. (The valve, like others used in this apparatus, was pneumatically actuated and remotely controlled.) The first metre of tubing leading from each transducer to its respective isolation valve was also housed in the enclosure.

Voltage-driven piezoelectric gas leak valves were used as the variable impedances Z_1, Z_2 and Z_3 (see figure 1). A mass flow controller was used as Z_2 for the majority of the measurements below the ambient temperature. It was replaced by the piezoelectric valve, which was slightly faster and allowed a greater dynamic range of flow.

The pressures p_1, p_2 and p_4 were controlled at their set-points by adjusting the voltage supplied to Z_1, Z_2 and Z_3 by a multi-channel digital voltage source. The voltages were updated by a discrete PID algorithm at a rate of approximately 1 Hz. Typically, the set-point for p_1 was fixed at 140 kPa while p_2 was stepped through the values 115 kPa, 120 kPa, 125 kPa, and 130 kPa. The resulting flow rates varied between $26\,\mu\mathrm{mol\,s^{-1}}$ and $73\,\mu\mathrm{mol\,s^{-1}}$. At each flow rate, p_4 was controlled sequentially at one of six different set points within the range 13 kPa to 75 kPa. At each $\{p_2, p_4\}$ combination, the system was given 20 min to achieve steady-state conditions. Figure 4 shows the stability of the four pressures for a helium flow through the two-capillary viscometer when both capillaries were at 298.15 K.

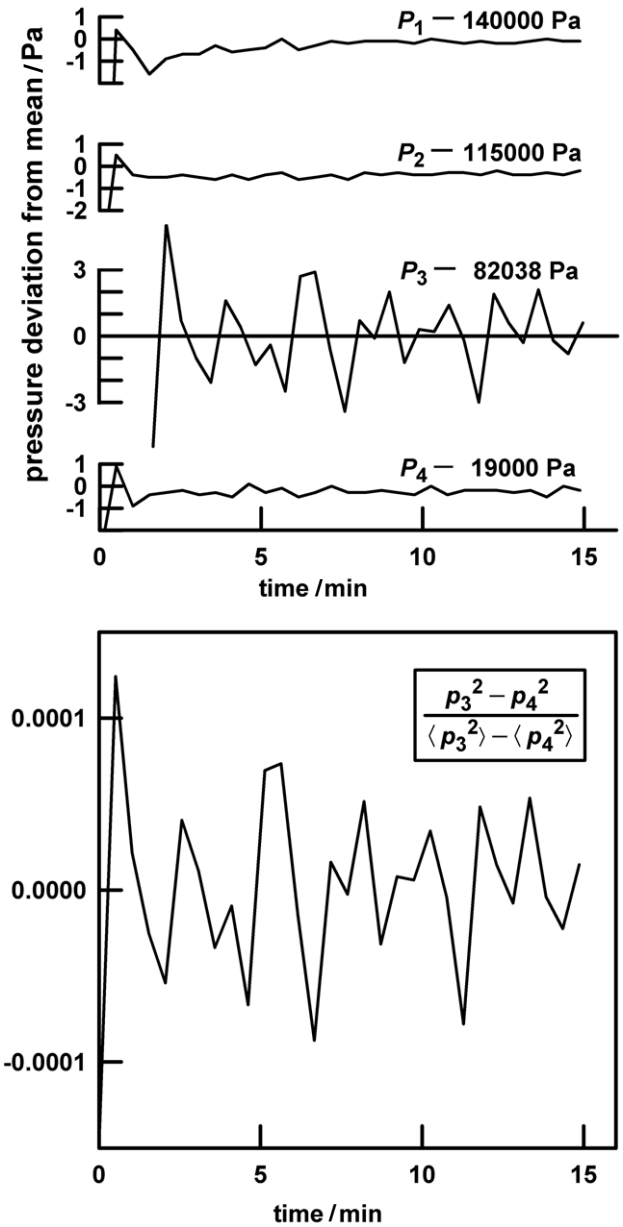

Figure 4. Top: time dependence of the pressures during a typical helium flow. Each curve is plotted relative to the pressure in the label, which is the mean pressure. The noise in the controlled pressures, p_1, p_2 and p_4, originated in the transducers and was less than 0.16 Pa, rms. Bottom: fractional fluctuations of $p_3^2 - p_4^2$ generated by noise in the uncontrolled pressure p_3. In this example, the rms fluctuation was 0.000 04 after the flow and the exit pressure stabilized.

To improve the stability of p_1 and p_4, gas-filled ballast volumes of 4 L and 0.5 L were connected just after Z_1 and just before Z_3, respectively. A bypass flow circuit was constructed from 6 mm ID stainless steel tubing so that each end of every high-impedance element (Z_1, Z_2, Z_3, $Z_{\mathrm{up},298}$ and $Z_{\mathrm{down,T}}$) within the viscometer could be rapidly evacuated. This bypass flow circuit was used also to flush the entire system with helium or argon (typically, three times) prior to the start of a run. After the first gas had been measured at each of the 24 $\{p_2, p_4\}$ combinations (four flow rates, six exit pressures), the viscometer was evacuated and flushed several times with the second gas, and then the 24 $\{p_2, p_4\}$ combinations were repeated. Each combination was maintained for 20 min and followed by a 3 min tare, and so a typical run at one temperature lasted 20 h. Evacuation, gas changing, flushing, flow control, taring and data acquisition were all automated.

The supplier of the helium stated its purity was 99.9999% by volume, and that it had a water content of less than 0.2 ppm. The supplier of the argon stated that its purity was 99.9995% by volume, with the dominant impurity being nitrogen. The gas impurity contributes an uncertainty that is an order of magnitude smaller than the other uncertainties in the present viscosity ratio measurements.

4. Analysis

The average values of the four pressures over the last 5 min of each 20 min flow period were converted to difference pressures ($\Delta p_{34} \equiv p_3 - p_4$, $\Delta p_{12} \equiv p_1 - p_2$) and mean pressures [$\bar{p}_{12} \equiv (p_1 + p_2)/2$, $\bar{p}_{34} \equiv (p_3 + p_4)/2$]. Each difference pressure was corrected by the tare value measured at the corresponding mean pressure. The nominal capillary dimensions were then used to calculate for every point the ratio

$$\Xi(T) \equiv \frac{\Delta p_{34}\bar{p}_{34}}{\Delta p_{12}\bar{p}_{12}} \frac{C^{\mathrm{gas}}(T, p_3, p_4)}{C^{\mathrm{gas}}(T, p_1, p_2)} = \frac{Z_{\mathrm{down,T}}}{Z_{\mathrm{up},298}} \frac{\eta^{\mathrm{gas}}_{0,T}}{\eta^{\mathrm{gas}}_{0,298}} \frac{T}{298.15\,\mathrm{K}}, \tag{13}$$

which corresponds to the quantity in square brackets in equation (8). For a given flow rate, adjusting all the values of $\bar{p}_{34}$ by +9 Pa decreased the scatter of the six values of $\Xi(T)$ corresponding to the six different exit pressures. Since this adjustment was within the experimental pressure uncertainty, it was applied to all the data reported here. (Adjusting $\bar{p}_{12}$ within its uncertainty did not have a similar effect.)

4.1. Calibration for flow-meter mode operation

When the temperature of both capillaries was 298.15 K, equation (13) reduced to $\Xi(298) = Z_{\mathrm{down},298}/Z_{\mathrm{up},298}$, allowing a calibration of the impedance ratio from pressure measurements. The first calibration used helium and indicated that $Z_{\mathrm{down},298}/Z_{\mathrm{up},298} = 0.999\,95$; thus, the capillaries were almost identical. To account for their slight difference, we increased L_{up} from its nominal value of 7.4520 m by 0.0004 m. This adjustment had a negligible effect on the value of $\Xi(T)$; it was convenient when using equation (8) to interpret the flow-meter mode data taken at temperatures other than 298.15 K.

Viscosity ratios were measured using the two-capillary viscometer over a period of eight months. During that period, six calibration runs, separated by at least several weeks, were conducted. With one exception, the impedance ratio $Z_{\mathrm{down},298}/Z_{\mathrm{up},298}$ decreased between calibrations. To account for the decreasing impedance ratio, we decreased the nominal value of r_{up} following each calibration. Consequently, r_{up} used in equations (5) and (8) decreased from 0.381 mm to its minimum value, 0.380 963 mm; this corresponds to a change of 0.000 38 in the impedance ratio. We speculate that the gradual decrease in r_{up} resulted from the accumulation of particles or of an oil film in this capillary although the gas from the supply cylinders always passed through particulate filters

before entering the capillaries. The exception to the gradual decrease in r_{up} occurred after a set of measurements during which the flow was reversed by interchanging the locations of the gas supply cylinders and the vacuum pump in figure 1.

The drifting impedance ratio limited the accuracy of data acquired in the flow-meter mode; however, it did not affect the data acquired in the helium-standard mode.

4.2. Parameters for the hydrodynamic model

Evaluation of the correction terms c_i^{gas} required six parameters for each fluid: the molar mass M, the zero-density viscosity $\eta_{0,T}^{gas}$, the density virial coefficient B_ρ, the thermal conductivity λ, the temperature derivative of the zero-density viscosity $d\eta_{0,T}^{gas}/dT$, and the viscosity virial coefficient $B_\eta \equiv \lim_{\rho\to 0}(\partial\eta/\partial\rho)_T$. (We ignored the third density and viscosity virial coefficients for helium and argon because the densities in this work were so low.) We calculated the parameters $\eta_{0,T}^{gas}$, B_ρ, λ and $d\eta_{0,T}^{gas}/dT$ from pair potentials and confirmed that the uncertainty of these parameters made a negligible contribution to the uncertainty of the measured viscosity ratios.

The viscosity virial coefficient B_η does make a significant contribution to the uncertainty budget (table 1); therefore, we consider it in some detail. The viscosity ratio measurements spanned a very limited pressure range (typically 43 kPa to 76 kPa); therefore, our results could not determine B_η for argon and helium. We instead used values deduced from published data. Since viscosity measurements are often reported as a function of pressure, we discuss the related quantity $b_T^{gas} \equiv \lim_{p\to 0}(\partial\eta/\partial p)_T/\eta$. The variation among sources in the literature of b_T^{gas} is of the order of 10% to 20%, for both helium and argon.

At 298 K, the values of b_T^{Ar} derived from the high-pressure viscosity data of Gracki *et al* [30], Evers *et al* [31], and Wilhelm and Vogel [32] have the average $(7.82 \pm 0.03) \times 10^{-9}\,Pa^{-1}$. The spread among the values of b_T^{Ar} deduced using the model of Rainwater and Friend and its most recent modification by Vogel *et al* is wider. Rainwater and Friend [33] report $8.8 \times 10^{-9}\,Pa^{-1}$; Vogel *et al* [34] report $6.8 \times 10^{-9}\,Pa^{-1}$. Therefore, we ignored the models and took b_T^{Ar} from the recent η–ρ–p–T correlation by Lemmon and Jacobsen [20], which takes into account a wide range of experimental data. We estimated the uncertainty of b_T^{Ar} from the consistency of the experimental references. At our coldest temperature (203 K), where the viscosity ratio is most sensitive to b_T^{Ar}, the values of b_{203}^{Ar} derived from references [20, 30–32] lie in the range $(14.2\text{–}16.6) \times 10^{-9}\,Pa^{-1}$. The corresponding fractional uncertainty of $\eta_{0,T}^{Ar}/\eta_{0,T}^{He}$ at 203 K is 0.000 10; it is smaller at higher temperatures.

At the temperatures used here, b_T^{He} is an order of magnitude smaller than b_T^{Ar}; its effect on the viscosity ratio is correspondingly smaller. At 298 K, the data of Gracki *et al* [30] give $b_{298}^{He} = -3.4 \times 10^{-10}\,Pa^{-1}$, the value derived from the 293.15 K data of Evers *et al* [31] is statistically indistinguishable from zero, and the Rainwater–Friend models [33–35] yield values from $-3.7 \times 10^{-10}\,Pa^{-1}$ to $-4.0 \times 10^{-10}\,Pa^{-1}$. At 203 K, the data of Gracki *et al* [30] differ from the Rainwater–Friend model [33] by only $9 \times 10^{-10}\,Pa^{-1}$. We used the data of Gracki *et al* [30] to estimate b_T^{He} at all temperatures; the corresponding uncertainty of $\eta_{0,T}^{Ar}/\eta_{0,T}^{He}$ is negligible.

In addition to the fluid parameters described above, the hydrodynamic model contains three constants that are fixed by theory (K_{ent}, K_{exp}, K_{therm}) and one constant (K_{slip}) that describes the degree of momentum accommodation at the capillary wall [9]. Our data for helium in the quartz capillary are consistent (independent of pressure) with the value $K_{slip} = 1.18$, which is similar to the values found previously [9]. For argon in the quartz capillary and for both gases in the nickel capillary, our results are consistent with $K_{slip} = 1.00$, which corresponds to complete momentum accommodation. For the two-capillary viscometer, we set $K_{ent} = 0$ because the matching bores of the T-unions and capillaries suppressed the kinetic energy change of gas entering the impedances. The values of K_{exp} and K_{therm} were the same as those used by Berg.

Four of the correction terms c_i^{gas} required an estimate of the Reynolds number. The initial values for these corrections were based on an estimate of $\dot{n}_0$, the molar flow-rate obtained without applying corrections to Poiseuille's law for a compressible fluid. Obtaining the final values required only three iterations of the model.

4.3. Capillary ellipticity and extrapolation to $De = 0$

Here, we consider the interaction of centrifugal effects (characterized by the Dean number) and the possibility that the nickel capillaries had a slightly elliptical cross section. For a given flow rate, the Reynolds and Dean numbers in the downstream capillary increased as the temperature decreased because of the decreasing gas viscosity. For helium, the maximum Dean number was 1.95 (corresponding to $Re = 32$); for the more dense argon, the maximum Dean number was 16.4 (corresponding to $Re = 265$). The hydrodynamic model extends to Dean numbers well in excess of 16 *if* the capillary bore is sufficiently circular and uniform [9]. In practice, the quartz capillaries met this criterion; however, the nickel capillaries did not.

We assumed that the capillary bore had a slightly elliptical cross section. From Srivastava's [36] analysis of this situation, we derived the lowest order correction to the centrifugal function f_{cent}.

$$\frac{f_{cent}(De, r/R_{coil}, \varepsilon)}{f_{cent}(De, r/R_{coil}, 0)} \approx 1 + K\,\varepsilon\,De^4. \qquad (14)$$

In equation (14), K is a constant given by the theory and $\varepsilon \equiv 1 - b/a$ is the flatness of an ellipse with (unknown) semi-radii a and b (see figure 6 of [9]). Equation (14) asserts that the apparent flow ratio $\dot{n}_{up,298}/\dot{n}_{down,T}$ (calculated from the measured pressures and the nominal capillary dimensions) is a linear function of De^4. Figure 5 shows that our data at 203 K, where the Dean number is largest, are indeed consistent with this assertion.

Our measured values of $R_{T,298}^{Ar,He}$ were obtained by evaluating $\Xi(T)$ for each gas in the limit $De \to 0$. Two extrapolation functions were tested. The first was a linear function of De that made no physical assumption. The second was a polynomial based on equation (14) that comprised a constant plus a term quartic in De; it assumed that deviations of $\Xi(T)$ were due to an elliptical cross section of the capillary. In cases where the Dean number was less than 11 (argon at $T > 298$ K and helium at all T), the difference between

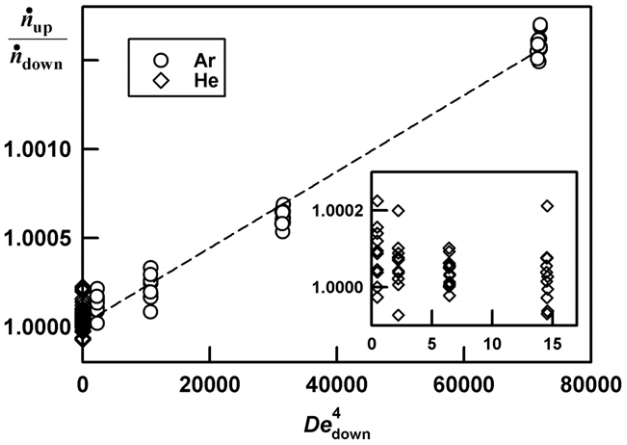

Figure 5. Apparent flow-rate ratio at 203 K (computed from the measured pressures and nominal capillary dimensions using equation (5)) as a function of De^4. The dashed line is a fit to the argon data.

the quartic fit and the linear fit was negligible (<0.0001). However, the difference was significant when the Dean number was larger. We investigated further by repeating the argon measurements at smaller De values near 212 K and 248 K. The original set had used $De < 16$; the repeated set, made several months later, used $De < 7$. As might be expected from figure 5, the quartic fit gave more consistent results: the values of $R^{Ar,He}_{T,298}$ determined by quartic extrapolation differed by no more than 0.000 13 between sets, whereas linear extrapolation led to differences as large as 0.000 59. Therefore, we evaluated $\Xi(T)$ in the limit $De \to 0$ at all temperatures by using the quartic function for argon.

We measured $R^{Ar,He}_{298,298} \equiv 1$ on five occasions and found the average to be $(0.999\,98 \pm 0.000\,04)$ when we extrapolated with the linear function, compared to $(0.999\,83 \pm 0.000\,04)$ with the quartic function. We are unable to explain this small inconsistency and, therefore, we estimate that the contribution to the uncertainty of $\eta^{Ar}_{0,T}/\eta^{He}_{0,T}$ from extrapolating to $De = 0$ is less than or equal to 0.000 17, despite having some evidence that the uncertainty is smaller at temperatures higher and lower than 298.15 K.

The measurements of the ratio of viscosity ratios have the empirical temperature dependence

$$R^{Ar,He}_{T,298} = 1.064\,65 - 0.720\,78\exp(-T/123.78\,\mathrm{K}); \quad 200\,\mathrm{K} < T < 400\,\mathrm{K}. \tag{15}$$

5. Results

5.1. Performance test: helium in flow-meter mode

Figure 6 compares our data for the viscosity ratio $\eta^{He}_{0,T}/\eta^{He}_{0,298}$ with the ratios calculated *ab initio* from the potential φ_B [6]. The data were obtained using the two-capillary viscometer in the flow-meter mode and they were analysed using equation (8). Thus, the comparison is limited by the stability of the impedance ratio $Z_{up,298}/Z_{down,298}$ between calibrations at 298.15 K and by our assumption that the thermal expansion of the downstream capillary is the same as that measured for pure nickel by Nix and McNair [21]. In the range 200 K to 400 K, the viscosity ratio varies from 0.77 to 1.21. The

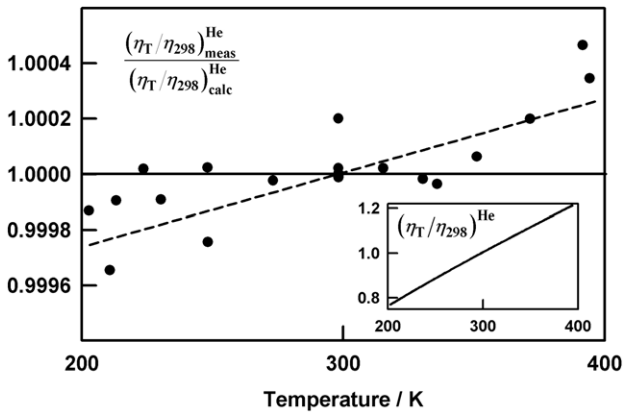

Figure 6. Comparison of the ratio $\eta^{He}_{0,T}/\eta^{He}_{0,298}$ measured using the two-capillary viscometer in flow-meter mode (equation (8)) with the ratio calculated from the *ab initio* potential φ_B [5,6] and published data for the thermal expansion of pure nickel [21]. If the thermal expansion of the nickel alloy capillaries were $0.9 \times 10^{-6}\,\mathrm{K}^{-1}$ larger than the literature data, the dashed line would become the baseline. Our results for $\eta^{Ar}_{0,T}$ and $\lambda^{Ar}_{0,T}$ use the helium-standard mode (equation (9)) and do not depend on the thermal expansion data. Inset: viscosity ratio as a function of temperature.

data depart fractionally from the calculated ratio by, at most, 0.000 45. This small difference is evidence that the two-capillary viscometer is well understood, even when operated over a fairly wide temperature range.

In figure 6, the dashed line indicates what would happen to the baseline if the thermal expansion of the downstream capillary exceeded the thermal expansion for pure nickel [21] by $0.9 \times 10^{-6}\,\mathrm{K}^{-1}$. The thermal expansion of pure nickel has an anomalous temperature dependence that peaks at its ferromagnetic Curie temperature (635 K). The Curie temperature changes with alloying and is sensitive to heat treatments; the thermal expansion is correspondingly sensitive.

Table 2 lists two ratios ($\eta^{He}_{0,T}/\eta^{He}_{0,298}$, $\eta^{Ar}_{0,T}/\eta^{Ar}_{0,298}$) measured with the two-capillary apparatus operating in flow-meter mode, together with their ratio, $R^{Ar,He}_{T,298} = (\eta^{Ar}_{0,T}/\eta^{He}_{0,T})/(\eta^{Ar}_{0,298}/\eta^{He}_{0,298})$, which is equivalent to operation in the helium-standard mode.

5.2. Results for viscosity ratios: helium-standard mode

Figure 7 compares our measurements of the viscosity ratio $\eta^{Ar}_{0,T}/\eta^{He}_{0,T}$ with other measurements and with calculations of the same ratio that used several argon–argon and helium–helium potentials. The baseline of figure 7 is equation (4), which fits the data with the rms deviation of 0.005%. The uncertainty of our ratio data is 0.024%.

In 1968 and 1969, Clarke and Smith [11,12] published two remarkable papers that included tabulated experimental values for $\eta^{Ar}_{0,T}/\eta^{N_2}_{0,T}$ and $\eta^{He}_{0,T}/\eta^{N_2}_{0,T}$ (as well as ratios for other gases). Figure 7 shows that their data (except for a single outlier that is not plotted) fall within 0.17% of our own.

Each smooth curve on figure 7 was computed from one argon–argon potential and one helium–helium potential. The solid curve that crosses our data used the potential of Boyes [18] for argon and φ_B from Hurly and Moldover [5] for helium. The dot–dash curve substitutes the helium potential φ_{00} for φ_B. This substitution moves the curve downwards 1.6 times the standard uncertainty of our data. In contrast, replacing Boyes'

Table 2. Ratio measurements made with the two-capillary viscometer. The relative standard uncertainty is 0.024%.

T/K	Flow-meter mode $\eta^{He}_{0,T}/\eta^{He}_{0,298}$	Flow-meter mode $\eta^{Ar}_{0,T}/\eta^{Ar}_{0,298}$	Helium-standard mode $R^{Ar,He}_{T,298}$
202.71	0.769 92	0.711 79	0.924 51
210.75	0.790 17	0.737 50	0.933 35
213.19	0.796 53	0.745 44	0.935 87
223.66	0.822 75	0.778 53	0.946 25
230.29	0.839 07	0.799 22	0.952 51
248.14	0.882 64	0.853 97	0.967 52
248.25	0.882 66	0.854 22	0.967 78
273.15	0.942 05	0.928 24	0.985 33
298.14	1.000 20	1.000 00	0.999 80
298.14	1.000 02	0.999 83	0.999 81
298.15	1.000 00	0.999 89	0.999 89
298.15	0.999 99	0.999 85	0.999 85
298.15	0.999 99	0.999 78	0.999 79
315.33	1.039 06	1.047 60	1.008 22
330.48	1.072 96	1.088 77	1.014 74
335.96	1.085 11	1.103 39	1.016 84
351.08	1.118 53	1.143 54	1.022 36
371.45	1.162 99	1.196 47	1.028 79
391.56	1.206 42	1.247 63	1.034 16
391.57	1.206 42	1.247 66	1.034 18
394.20	1.211 88	1.254 15	1.034 88

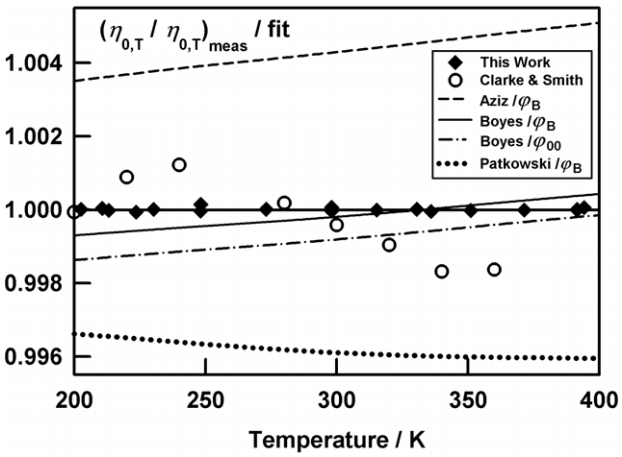

Figure 7. Comparison of the ratio $\eta^{Ar}_{0,T}/\eta^{He}_{0,T}$ measured in this work with the ratio calculated from various argon–argon and helium–helium potentials. The baseline is equation (4). Our data agree best with the ratio calculated from Boyes' [18] potential for argon and φ_B for helium from [5].

argon potential with that of Aziz [19] or the *ab initio* argon–argon potential of Patkowski *et al* [37] has a much greater effect. Thus, the present data have the power to discriminate between sophisticated models of the argon–argon potential.

5.3. Results for the viscosity of argon: helium-standard mode

The third column of table 3 presents values of $\eta^{Ar}_{0,T}$ deduced from our measurements in the helium-standard mode, i.e. analysed using equation (9). We used the helium-standard mode because this mode does not rely on the literature value of nickel's thermal expansion or upon the stability of the impedance ratio $Z_{down,298}/Z_{up,298}$. In section 7, we compare our values of $\eta^{Ar}_{0,T}$ with the correlation by Lemmon and Jacobsen [20].

Table 3. Argon's transport properties at zero density. The relative standard uncertainty is 0.024% for the viscosity ratio and 0.084% for the viscosity and thermal conductivity.

T/K	$\eta^{Ar}_{0,T}/\eta^{He}_{0,T}$	$\eta^{Ar}_{0,T}$/μPa s	$\lambda^{Ar}_{0,T}$/mW m^{-1} K^{-1}
202.71	1.052 09	16.075	12.557
210.75	1.062 15	16.660	13.013
213.19	1.065 02	16.835	13.150
223.66	1.076 84	17.581	13.734
230.29	1.083 96	18.050	14.101
248.14	1.101 04	19.284	15.067
248.25	1.101 33	19.294	15.075
273.15	1.121 31	20.962	16.381
298.14	1.137 77	22.577	17.646
298.14	1.137 79	22.577	17.646
298.15	1.137 87	22.579	17.648
298.15	1.137 83	22.578	17.647
298.15	1.137 76	22.577	17.646
315.33	1.147 36	23.656	18.492
330.48	1.154 78	24.586	19.221
335.96	1.157 16	24.916	19.481
351.08	1.163 44	25.821	20.189
371.45	1.170 76	27.012	21.124
391.56	1.176 87	28.160	22.025
391.57	1.176 90	28.161	22.025
394.20	1.177 69	28.312	22.143

6. Thermal conductivity of argon

We require values of the Prandtl number to calculate $\lambda^{Ar}_{0,T}$ using equation (3). Here, we discuss the source of these values and we estimate their uncertainty.

Hirshfelder *et al* [38] provide algorithms for calculating the transport properties of a gas at zero pressure from intermolecular potentials. In the lowest order approximation, the Prandtl number at zero pressure is 2/3 for the monatomic gases, independent of the intermolecular potential. Higher approximations yield values for the Prandtl number that have a weak dependence on the potential, as illustrated by the results for six potentials in figure 8. The dotted line (hard-sphere potential) and the dashed curve (Lennard-Jones potential) were calculated by Viehland *et al* [39]. (We scaled Viehland *et al*'s Lennard-Jones results using $\varepsilon/k_B = 124$ K for argon.) The solid curve represents the values of the Prandtl number that we calculated from four, more accurate, potentials. They are (1) the three-parameter potential by Maitland and Smith [40], (2) the multiparameter potentials developed by Aziz [19], (3) Boyes' modification of the Aziz potential to account for speed-of-sound data [18], and (4) the potential constructed *ab initio* by Patkowski *et al* [37]. In figure 8, the results for these four potentials are indistinguishable from the solid curve in the third, fourth and fifth order approximations for the transport properties. The effects of adding quantum corrections to the calculation are also too small to be detected on the figure. A convenient representation of the fifth order result from the Boyes potential is

$$Pr = 0.658\,155 + 0.210\,68(T/\mathrm{K})^{-1/2} - 1.379\,75(T/\mathrm{K})^{-1}, \quad 200\,\mathrm{K} < T < 400\,\mathrm{K}. \tag{16}$$

We estimated that the fractional uncertainty of the Prandtl number for argon at 200 K is 0.000 04 from the maximum difference among the four more accurate potentials. The uncertainty is lower at higher temperatures.

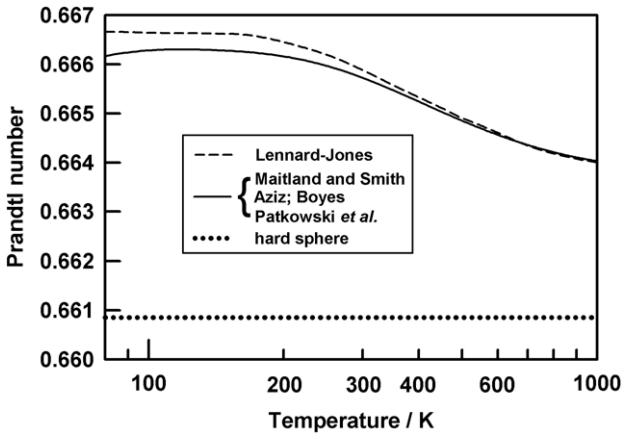

Figure 8. Prandtl number of argon computed from various model potentials.

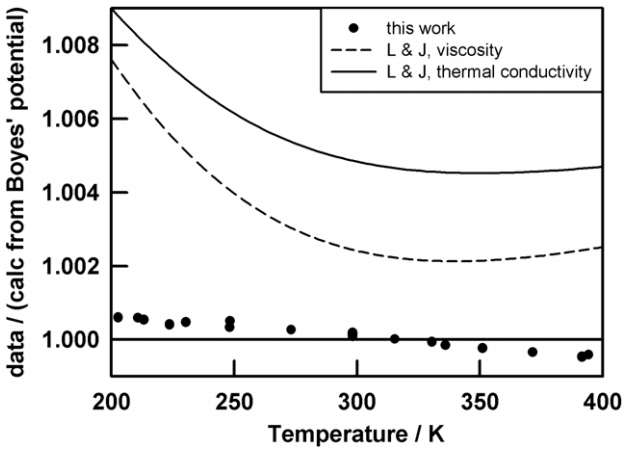

Figure 9. Ratio of measured transport properties of argon to those calculated from Boyes' potential [18]. The plotted points (this work) for the thermal conductivity and viscosity are superimposed because our values for the Prandtl number (equation (16)) came from fits to Boyes' results. The curves represent Lemmon and Jacobsen's extensive correlation of experimental data [20].

Table 3 lists the values of the thermal conductivity of argon at zero pressure. The relative uncertainty of 0.000 84 is the sum in quadrature of the terms in table 1. In section 7, we compare our values of $\lambda_{0,T}^{Ar}$ with the correlation by Lemmon and Jacobsen [20].

7. Discussion

In 2004, Lemmon and Jacobsen (L & J) reviewed and correlated the extensive experimental data for the viscosity and the thermal conductivity of argon [20]. Their $\eta_{0,T}^{Ar}$ and $\lambda_{0,T}^{Ar}$ results are available in a user-friendly computer program [41]. At low densities, L & J graphically compared their correlation of the viscosity of argon with 47 of 71 primary data sources. They also compared their correlation of the thermal conductivity of argon with 47 of 62 primary data sources. Due to this plethora of primary sources, we use figure 9 to compare our results to the L & J correlation. Figure 9 uses values of $\eta_{0,T}^{Ar}$ and $\lambda_{0,T}^{Ar}$ computed from Boyes' potential [18] as a baseline.

In figure 9, our plotted points for the thermal conductivity and viscosity are superimposed because our values for $\lambda_{0,T}^{Ar}$ were calculated using equation (16) for the Prandtl number and equation (16) is a fit to values of the Prandtl number calculated from Boyes' potential. The curves in figure 9 represent the correlation of L & J. Near 300 K, our viscosity values are 0.2% smaller than the values from L & J. This difference grows to 0.7% near 200 K. This difference is reasonable considering that L & J estimated the uncertainty of their viscosity correlation to be 0.5% at low densities. L & J's viscosity-deviation plot (their figure 2) spans ±2%. Near 300 K, our thermal conductivity values are 0.5% smaller than the values from the L & J correlation and this difference becomes 0.9% near 200 K. These differences are consistent with L & J's estimate that the uncertainty of the thermal conductivity correlation is 2% at a low density. L & J's thermal conductivity deviation plot (figure 10 of reference [20]) spans ±5%.

The contrast between the L & J correlation (2% uncertainty of $\lambda_{0,T}^{Ar}$) and the present results (0.08% uncertainty of $\lambda_{0,T}^{Ar}$) suggests that future correlations for the noble gases anchor $\lambda_{0,T}^{gas}$ to the values obtained by combining viscosity measurements with the Prandtl number computed from a model potential.

The remarkable agreement between the present viscosity ratio measurements and those of Clarke and Smith (figure 7) leads us to recommend the routine use of viscosity ratio measurements with helium as a standard to determine the viscosity of gases at low densities.

Acknowledgments

The authors are grateful to Laurent Pitre, who helped design and construct the flow control system, Roberto Gavioso for assistance with several measurements, John Wright for equipment loans and flow calibrations, and Greg Strouse and Dawn Cross for calibrating the thermometers. Allan Harvey, Eric Lemmon, and Dean Ripple gave helpful reviews of the manuscript. While at NIST, EFM was supported in part by an AAA/ANZ Education Fellowship.

References

[1] Moldover M R, Boyes S J, Meyer C W and Goodwin A R H 1999 *J. Res. NIST* **104** 11
[2] Strouse G F, Defibaugh D R, Moldover M R and Ripple D C 2003 *Temperature: Its Measurement and Control in Science and Industry* vol VII (8th International Temperature Symposium, Chicago, IL, 21–24 October 2002) ed D C Ripple (American Institute of Physics) pp 31–6
[3] Moldover M R, Trusler J P M, Edwards T J, Mehl J B and Davis R S 1988 *J. Res. Natl. Bur. Stand* **93** 85
[4] Fellmuth B, Fischer J, Gaiser C and Buck W 2005 BIPM Document CCT/05-02 http://www.bipm.fr/cc/CCT/Allowed/23/CCT_05_02.pdf
[5] Hurly J J and Moldover M R 2000 *J. Res. Natl. Inst. Stand. Technol.* **105** 667
[6] Hurly J J and Moldover M R 2004 unpublished Hurly J J and Mehl J B in preparation
[7] Kestin J and Leidenfrost W 1959 *Physica* **25** 1033–62
[8] Evers C, Lösch H W and Wagner W 2002 *Int. J. Thermophys.* **23** 1411
[9] Berg R F 2005 *Metrologia* **42** 11
[10] Berg R F 2006 *Metrologia* **43** 183 (Erratum)

[11] Clarke A G and Smith E B 1969 *J. Chem. Phys.* **51** 4156
[12] Clarke A G and Smith E B 1968 *J. Chem. Phys.* **48** 3988
[13] Dawe R A and Smith E B 1969 *J. Chem. Phys.* **52** 693
[14] Guevara F A, McInteer B B and Wageman W E 1969 *Phys. Fluids* **12** 2493
[15] Gough W W, Matthews G P and Smith E B 1976 *J. Chem. Soc. Faraday Trans. I* **72** 645
[16] Camani M 1970 *Helv. Phys. Acta* **44** 437
[17] Russell P A, Buffham B A, Mason G, Richardson D J and Heslop M J 2004 *Fluid Phase Equilib.* **215** 195
Russell P A, Buffham B A, Mason G and Heslop M J 2005 *Chem. Eng. Sci.* **60** 2943
[18] Boyes S J 1994 *Chem. Phys. Lett.* **221** 467
[19] Aziz R A 1993 *J. Chem. Phys.* **99** 4518
[20] Lemmon E W and Jacobsen R T 2004 *Int. J. Thermophys.* **25** 21
[21] Nix F C and MacNair D 1941 *Phys. Rev.* **60** 597
[22] Cencek W, Jeziorska M, Bukowski R, Jaszunski M, Jeziorski B and Szalewicz K 2004 *J. Phys. Chem.* A **108** 3211
[23] Gdanitz R J 2001 *Mol. Phys.* **99** 923
[24] Komasa J J 2001 *Chem. Phys.* **115** 158
[25] Zwillinger D (ed) 1996 *Standard Mathematical Tables and Formulae* (Boca Raton, FL: CRC Press) section 7.8.1.2
[26] Taylor B N and Kuyatt C E 1994 *Guidelines for evaluating and expressing the uncertainty of NIST measurement results* NIST Technical Note 1297
[27] Wright J D, Johnson A N and Moldover M R 2003 *J. Res. Natl. Inst. Stand. Technol.* **108** 21
[28] Wilhelm J, Gillis K A, Mehl J B and Moldover M R 2000 *Int. J. Thermophys.* **21** 983
[29] Berg R F 2004 *Rev. Sci. Instrum.* **75** 772–9
[30] Gracki J A, Flynn G P and Ross J 1969 *J. Chem. Phys.* **51** 3856
[31] Evers C, Lösch H W and Wagner W 2002 *Int. J. Thermophys.* **23** 1411
[32] Wilhelm J and Vogel E 2000 *Int. J. Thermophys.* **21** 301
[33] Rainwater J C and Friend D G 1987 *Phys. Rev.* A **36** 4062
[34] Vogel E, Küchenmeister C, Bich E and Laesecke A 1998 *J. Phys. Chem. Ref. Data* **27** 947
[35] Bich E and Vogel E 1991 *Int. J. Thermophys.* **12** 27
[36] Srivastava R S 1980 *J. Appl. Math. Phys.* **31** 297
[37] Patkowsi K, Murdachaew G, Fou C-M and Szalewicz K 2005 *Mol. Phys.* **103** 2031–45
[38] Hirschfelder J O, Curtiss C F and Bird R B 1964 *Molecular Theory of Gases and Liquids* (New York: Wiley)
[39] Viehland L A, Janzen A R and Aziz R A 1995 *J. Chem. Phys.* **102** 5444
[40] Maitland G C, Rigby M, Smith E B and Wakeham W A 1981 *Intermolecular Forces* (Oxford: Clarendon Press) pp 497–8. For argon, the parameters of the Maitland–Smith potential are $\gamma = 9$, $\varepsilon = 142.1$ and $r_m = 3.76$
[41] Lemmon E W, McLinden M O and Huber M L 2002 *Reference Fluid Thermodynamic and Transport Properties*, NIST Standard Reference Database 23, Version 7.0